COMPUTATIONAL SCIENCE AND TECHNIQUES
Volume 10, 2026, 692-701

Publisher: Klaipėda University
https://computational.online
Online ISSN: 2029-9966
DOI: 10.15181/csat.v10.2602

POWER-BALANCE ASSESSMENT OF PEMFC–BATTERY–PV HYBRID ARCHITECTURES FOR A ROUTE-INSPIRED PROTOTYPE CATAMARAN

Aya A. ElBauomy[1], Gintvilė Šimkonienė[2], Mostafa Ahmed Abdelgeliel[1], Kareem M. Tonbol[1]

[1]Arab Academy for Science, Technology and Maritime Transport, Alexandria, Egypt
[2]Faculty of Marine Technology and Natural Sciences, Klaipėda University, Lithuania

Abstract

Maritime decarbonization requires propulsion systems that are low-emission and dynamically suitable for repeated short-route operation. This paper presents a route-inspired, time-domain power-balance assessment of proton exchange membrane fuel cell (PEMFC)-based hybrid architectures for a 1.80 m prototype catamaran. A real ferry operating context in the Suez Canal region was translated into a representative 15 min prototype operating cycle repeated over an 8 h operating window. Three cases were evaluated under the same DC-bus load basis: Case 1, PEMFC + Battery; Case 2, PEMFC + PV; and Case 3, PEMFC + PV + Battery. The PEMFC-battery calculations were based on DC-bus power balance, converter, battery-current, and SOC equations, while the PV contribution was calculated using a shipboard PV power model with PVGIS seasonal irradiance and temperature inputs. The results show that Case 1 eliminates repeated startup deficits through battery support, whereas Case 2 reduces PEMFC loading but cannot remove startup deficits without an energy buffer. Under the best seasonal PV input, July, the PV peak reached 84.88 W, and the PV-used energy in Case 2 was 399.64 Wh. Case 3 increased the utilized PV-bus energy to 450.87 Wh, maintained the final SOC at 0.90, and removed the repeated transient deficits under the adopted ideal power-balance assumptions. Therefore, the PEMFC + PV + Battery architecture is selected as the preferred configuration for the next phase of experimental prototyping.

Keywords: PEMFC; battery; photovoltaic; hybrid propulsion; DC-bus power balance.

Introduction

Maritime decarbonisation is increasingly important for coastal and inland-waterway operations, where vessels operate close to populated areas, and their emissions directly affect local air quality, public health, and noise levels. Ship emissions include CO_2, NOx, SOx, particulate matter, and volatile organic compounds, and previous studies have highlighted their impact on coastal and port cities, including respiratory and cardiovascular health effects (Bassam *et al.*, 2023; IMO, 2023). Therefore, short-route vessels such as ferries are important candidates for zero- and low-emission propulsion systems.

At the global level, the maritime sector is under pressure to reduce greenhouse gas emissions and move toward zero-emission energy systems (Vahabzad, Mohammadi-Ivatloo, and Anvari-Moghaddam, 2021; IMO, 2023). The Suez Canal region is also strategically relevant to this transition. It is not only a major maritime route, but has also been discussed as a potential green corridor and hydrogen-related hub linking Europe, the Middle East, and Asia (Ringel *et al.*, 2024; Zumbraegel and Kegel, 2025). In the local context, the Port Said–Port Fouad ferry route provides a practical short-route case: previous work reports that Suez Canal ferries operate between the

two canal banks, with the route distance around 1 km, an average voyage time of 7 min, and about 8 min for loading and unloading (Bassam *et al.*, 2023).

Hydrogen PEM fuel cells are a promising solution for clean marine electrification, especially when combined with batteries and renewable energy sources (Balestra and Schjølberg, 2021; Cha *et al.*, 2021; Zhaka and Samuelsson, 2024). In hybrid PEMFC–battery systems, the battery can supply fast transient power and can also be charged during suitable operating periods, while the fuel cell provides the main continuous power. Previous shipboard PEMFC–battery studies show that the energy management system is responsible for controlling the power flows between the fuel cell, battery, converters, and load (Balestra and Schjølberg, 2021). Solar PV can further reduce the fuel-cell burden during daylight operation, particularly in Egypt, where solar energy potential is high, and PV systems are suitable for maritime and shore-side applications (Vahabzad, Mohammadi-Ivatloo, and Anvari-Moghaddam, 2021; Bassam *et al.*, 2023; Kumar and Kanimozhi, 2024).

Although many studies have investigated the simulation and optimisation of hybrid ship power systems, practical EMS validation remains necessary before implementation (Balestra and Schjølberg, 2021; Kumar and Kanimozhi, 2024). Real converters, batteries, PEMFC stacks, sensors, and hydrogen-supply components introduce losses and dynamic behaviour that cannot be fully captured in an ideal numerical model. Therefore, this paper represents the computational phase of a broader laboratory-prototype research pathway. A 1.80 m catamaran prototype is used as a small-scale platform, and three PEMFC-based architectures are compared under the same route-inspired 15 min operating cycle repeated over an 8 h window: PEMFC + Battery, PEMFC + PV, and PEMFC + PV + Battery. The aim is to identify the most suitable architecture for the next experimental EMS phase.

2. Methodology

2.1 Prototype mission basis

The representative operating cycle is 15 min and is repeated over an 8-h operating day (Bassam *et al.*, 2023). The number of repeated cycles is calculated as:

$$N_{cyc} = \frac{T_{OP}}{T_{cyc}} \tag{1}$$

where N_{cyc} is the number of repeated operating cycles, T_{OP} is the total operating duration, and $T_{cyc}$is the duration of one representative prototype cycle. In this study, T_{OP} = 8 h and T_{cyc} = 15 min = 0.25 h; therefore, the 8 h operation contains 32 repeated cycles.

The time-domain power-balance model was implemented in MATLAB R2025b using a script-based simulation approach rather than Simulink. All calculations were performed numerically at each time step according to the adopted DC-bus power-balance equations. The mission phases and load levels used in the MATLAB script are summarised in Table 1.

2.2 DC-bus load formulation

Because the propulsion motors operate at 12 V while the selected PEMFC stack and battery branch are represented at the common DC bus, the source-side demand includes propulsion power, drive/converter losses, and auxiliary electrical load:

$$P_{dem}(t) = \frac{P_{prop}(t)}{\eta_{drive}} + P_{aux} \tag{2}$$

where $P_{dem}(t)$ is the total electrical demand at the DC-bus level, $P_{prop}(t)$ is the propulsion-side demand, η_{drive} is the representative drive/converter efficiency, and P_{aux} is the auxiliary electrical load. Using η_{drive} = 0.90 and an auxiliary load of approximately 25 W, the baseline cruise demand is represented as approximately 240 W, while the startup demand reaches approximately 398 W.

Table 1. Prototype mission and simulation parameters

Item	Value	Role in model
Length overall, *LOA*	1.80 m	Prototype scale definition
Length at waterline, *LWL*	1.67 m	Prototype hull reference
Moulded depth, *D*	0.41 m	Prototype geometry reference
Draft, *T*	0.17 m	Prototype operating condition
Operating window	8 h	Repeated daily simulation period
Cycle duration	15 min	Representative prototype mission cycle
Number of cycles	32	Repeated cycles over 8 h
DC-bus voltage	24 V	Common electrical bus basis
PEMFC power limit	200 W	Fuel-cell power limit
Battery support limit	±240 W	Charge/discharge branch limit
Battery capacity	5 Ah	SOC and C-rate calculation basis
SOC limits	0.25–0.90	Battery operating window
Phase load levels	398 W; 314 W; 240 W; 269 W; 25 W	Startup, acceleration, cruise, manoeuvring, low-load

2.3 Reference-based DC-bus power-balance model

The investigated architectures are represented using a common DC-bus power-balance framework adapted from published PEMFC–battery ship models. The DC-bus balance, PEMFC converter power, battery charge/discharge relation, battery current, and SOC update follow the formulation of (Wu, Partridge, and Bucknall, 2020), while the marine hybrid power-plant load-sharing context is supported by (Balestra and Schjølberg, 2021). The generalized bus-level balance is written as:

$$P_1(t) + P_2(t) + P_{PV}(t) + P_s(t) = P_{dem}(t) \quad (3)$$

where $P_1(t)$ is the PEMFC power delivered to the DC bus, $P_2(t)$ is the signed battery branch power at the DC bus, $P_{PV}(t)$ is the PV power injected into the DC bus, $P_s(t)$ is shore power, and $P_{dem}(t)$ is the total load demand. Positive $P_2(t)$ denotes battery discharge, while negative $P_2(t)$ denotes battery charging. In the present operating simulation, shore power is not included; therefore, $P_s(t) = 0$. (4)

$$P_s(t) = 0$$

where $P_s(t)$ is the shore-power contribution. In the present operating simulation, shore power is not used during the 8 h mission window; therefore, $P_s(t)$ is set to zero.

$$P_2(t) = P_{dem}(t) - P_1(t) - P_{PV}(t) - P_s(t) \quad (5)$$

where $P_2(t)$ is the required battery branch power at the DC-bus level. When $P_2(t) > 0$, the battery supplies the remaining load demand. When $P_2(t) < 0$, surplus power is available, and the battery is charged. In the prototype simulation, P_2 *(t)* is constrained by the selected battery support limit of ±240 W.

$$P_1(t) = P_{fc}(t) \cdot \eta_1 \tag{6}$$

where $P_1(t)$ is the PEMFC power delivered to the DC bus. $P_{fc}(t)$ is the PEMFC output power before the converter, and $\eta_1$is the PEMFC converter efficiency. In this preliminary power-balance simulation, η_1 is set to unity to isolate the effect of the selected source power ratings.

$$P_2 = \begin{cases} P_{bat}(t) \cdot \eta_2, for discharge \\ P_{bat}(t) / \eta_3, for charge \end{cases} \tag{7}$$

where $P_{bat}(t)$ is the battery-side power, P_2 *(t)* is the battery branch power at the DC bus, η_2 is the battery discharge converter efficiency, and η_3 is the battery charge converter efficiency. The discharge mode is used when the battery supplies the DC bus, while the charge mode is used when surplus source power is directed to the battery.

$$P_{bat} = I_B \cdot V_B \tag{8}$$

where P_{bat} is the battery-side power, I_B is the battery current, and V_B is the battery voltage. A positive current represents battery discharge, while a negative current represents battery charging.

$$\Delta SOC = -\eta_b \int_{t_1}^{t_2} C(t)dt \tag{9}$$

where ΔSOC is the change in battery state of charge over the interval from t_1 to t_2, η_b is the battery coulombic efficiency, and $C(t)$ is the battery C-rate. This formulation links the battery C-rate to the SOC variation over time.

$$SOC(k+1) = SOC(k) - \eta_b \cdot [\, I_B(k) \,/\, Q_{batt} \,] \cdot \Delta t \,/\, 3600 \tag{10}$$

where *SOC(k)* is the battery state of charge at time step k, $I_B(k)$ is the battery current, Q_{batt} is the nominal battery capacity in ampere-hours, η_b is the battery coulombic efficiency, and Δt is the simulation tiType equation here.me step in seconds. The factor 3600 converts seconds to hours. The *SOC* is constrained between SOC_{min} = 0.25 and SOC_{max} = 0.90.

$$P_{tot}(t) = n_{fc} \cdot P_1(t) + n_{batt} \cdot P_2(t) + P_{PV}(t) \tag{11}$$

where P_{tot}(t) is the total supplied power at the DC-bus level, n_{fc} is the number of PEMFC units, n_{batt} is the number of battery branches, $P_1(t)$ is the delivered PEMFC power, $P_2(t)$ is the signed battery branch power, and P_{PV} (t) is the PV power injected into the DC bus. For the present prototype, n_{fc} = 1 and n_{batt} = 1 when the battery branch is included. In Case 2, the battery branch is removed, so $n_{batt}P_2(t) = 0$:

$$P_{def}(t) = max[\,0,\ P_{dem}(t) - P_{tot}(t)] \tag{12}$$

where P_{def}(t) is the instantaneous unmet load. A zero value indicates that the selected architecture satisfies the load demand under the adopted power-balance assumptions.

2.4 Reference-based PV model and case definitions

The PV contribution in Cases 2 and 3 is calculated using the shipboard solar-generation formulation adapted from (Vahabzad, Mohammadi-Ivatloo, and Anvari-Moghaddam, 2021). The available PV power is:

$$P_{PV,av}(t) = \sigma_\theta \cdot \sigma_k \cdot \eta_{PV,conv} \cdot \eta_{PV}(t) \cdot A_{PV} \cdot G(t) \tag{13}$$

here $P_{PV,av}(t)$ is the available PV power, $G(t)$ is the solar irradiance, A_{PV} is the installed PV surface area, $\eta_{PV,conv}$ is the PV converter efficiency term, $\eta_{PV}(t)$ is the PV panel efficiency, σ_k is the dirtiness coefficient, and σ_θ is the operating correction coefficient. In this study, $G(t)$ is taken from PVGIS seasonal irradiance data for the selected route location.

$$\eta_{PV}(t) = \eta_{PV,ref} \cdot \eta_T \cdot [1 - \tau \cdot (T_C(t) - T_{C,ref})] \tag{14}$$

where $\eta_{PV}(t)$ is the temperature-corrected PV efficiency, $\eta_{PV,ref}$ is the reference PV efficiency, η_T is the tracking efficiency, τ is the temperature coefficient, $T_C(t)$ is the PV cell temperature, and $T_{C,ref}$ is the reference cell temperature. For the fixed prototype PV installation, η_T is taken as unity.

$$T_C(t) = T_a(t) + [(NOCT - 20)/800]\, G(t) \tag{15}$$

where $T_C(t)$ is the PV cell temperature, $T_a(t)$ is the ambient temperature, $NOCT$ is the normal operating cell temperature, and $G(t)$ is the solar irradiance. In this study, $T_a(t)$ is taken from PVGIS ambient-temperature data for latitude/longitude 31.258 and 32.303 (PVGIS, 2026).

$$0 \le P_{PV}(t) \le P_{PV,max} \tag{16}$$

where $P_{PV,max}$ is the installed rated PV power. This constraint prevents the calculated PV power from becoming negative or exceeding the rated capacity of the installed PV module. In the present prototype simulation, $P_{PV,max}$ = 100 W.

Three architectures are evaluated from the generalized DC-bus balance. In Case 1, PEMFC + Battery, the PV branch is not included; therefore, $P_{PV}(t) = 0$. In Case 2, PEMFC + PV, the battery branch is removed; therefore, $P_2(t) = 0$. In Case 3, PEMFC + PV + Battery, both the PV and battery branches are active. The dispatch priority is prototype-specific: PV serves the load first, the PEMFC supplies the residual demand up to the selected 200 W limit, the battery supplies any remaining transient demand, and surplus PV can charge the battery when the *SOC* is below its upper limit. This EMS priority is not introduced as a reference-paper equation; it is the operating rule of the prototype model. The resulting power-flow calculations follow the reference-based equations above.

3. Results

3.1 Case 1: PEMFC + Battery power-balance simulation

Case 1 confirms the role of the battery as the transient-support branch. During startup, the load reaches 398 W. With the PEMFC limited to 200 W, the battery supplies approximately 198 W, which remains below the selected ±240 W battery limit. During acceleration, cruise, and manoeuvring, the battery supplies approximately 114 W, 40 W, and 69 W, respectively. The net supplied power follows the repeated load profile with approximately zero deficit under the adopted ideal power-balance assumptions. This case demonstrates that the PEMFC + Battery architecture is dynamically adequate for the representative mission, but it does not benefit from solar energy support.

3.2 Case 2: PEMFC + PV

Case 2 evaluates whether PV support can replace the battery branch. The best seasonal PV input was obtained in July (shown in Fig. 1). Under this condition, the PV peak reached 84.88 W, and the PV-used energy over the 8 h operating window was 399.64 Wh. The PV branch reduces PEMFC loading during cruise and low-load periods. For example, when the load is approximately 240 W, the PV contribution reduces the PEMFC requirement below the 200 W limit.

However, Case 2 cannot fully satisfy the repeated startup and acceleration phases. During startup, the demand is 398 W. Even when the PEMFC provides 200 W, and PV contributes approximately 84.88 W near the best solar condition, the available supplied power is about 284.88 W. Therefore, a startup deficit of approximately 113 W remains. This repeated deficit appears at the beginning of each 15 min cycle. The result shows that PV is useful for reducing the PEMFC energy burden, but it cannot replace the fast transient-support function of the battery.

The seasonal Case 2 results show that July provides the strongest PV contribution, with 399.64 Wh of PV energy used compared with 257.75 Wh in January. However, even under this favourable solar condition, the architecture still has 51.23 Wh of unmet load and a maximum deficit of 161.52 W because it lacks a battery branch to support repeated startup and acceleration transients. Therefore, PV reduces the PEMFC burden, but it cannot replace the transient buffering function of the battery.

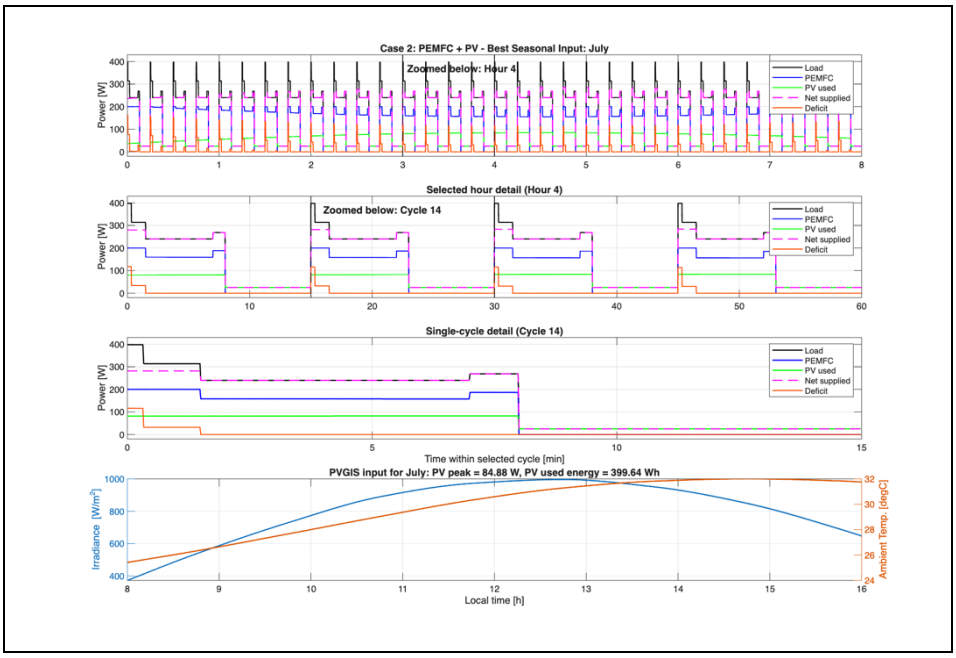

Figure 1. Case 2 PEMFC + PV simulation under the best seasonal PV input, July

3.3 Case 3: PEMFC + PV + Battery

Case 3 combines the two support mechanisms (shown in Fig. 2). The PV branch reduces PEMFC loading when solar power is available, while the battery branch covers the residual transient demand. Under the July PV input, the PV peak remains 84.88 W, but the utilised PV-bus energy increases to 450.87 Wh because part of the PV surplus can be directed to the battery during low-load intervals. The final SOC remains at 0.9 indicating that the battery returns to its upper operating limit by the end of the selected operating window.

During startup, the combined PEMFC and PV contribution is still lower than the 398W demand, but the battery supplies the remaining difference. During the cruise, the PV contribution reduces the PEMFC requirement, and during low-load periods, the battery may be charged from surplus PV. As a result, the net supplied power follows the operational load, and the deficit remains approximately zero. This confirms that the integrated PEMFC + PV + Battery architecture provides the most balanced response among the three cases: the PEMFC provides the main continuous supply, PV reduces the PEMFC burden, and the battery provides transient support and short-term energy buffering.

Conclusion

This paper presented a reference-based time-domain power-balance assessment of three PEMFC-based hybrid architectures for a 1.80 m prototype catamaran operating over a repeated short-route mission. The mission was represented by a 15 min operating cycle repeated over an 8 h window. The PEMFC-battery calculations were based on published DC-bus power-balance, converter, battery-current, and SOC equations. At the same time, the PV contribution was calculated using a shipboard PV formulation with PVGIS seasonal irradiance and ambient-temperature data.

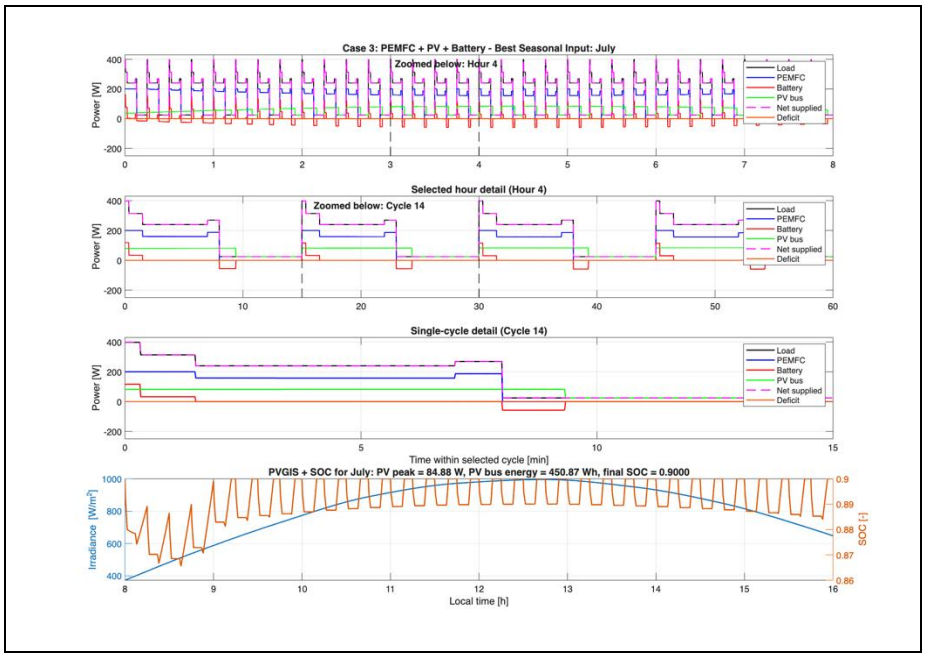

Figure 2. Case 3 PEMFC + PV + Battery simulation under the best seasonal PV input, July.

The results show that Case 1, PEMFC + Battery, is dynamically capable of following the representative load profile because the battery supplies the startup and transient residual demand. Case 2, PEMFC + PV, reduces the PEMFC loading during solar availability but cannot eliminate the repeated startup deficit because no energy-storage branch is available. Under the best seasonal input in July, the PV peak reached 84.88 W, and the PV–used energy was 399.64 Wh, but a startup deficit remained. Case 3, PEMFC + PV + Battery, provided the most balanced response. It increased the utilised PV-bus energy to 450.87 Wh, maintained the final SOC at 0.90, and eliminated the repeated transient deficit under the adopted ideal power-balance assumptions.

The results should be interpreted as a preliminary computational screening stage under ideal power-balance assumptions. The use of unity converter efficiencies and simplified source dynamics may slightly overestimate the power available at the DC bus. Therefore, the unmet load in Case 2 could be higher in experimental operation, while the battery discharge demand in Case 3 could increase, and the final SOC could become lower than the ideal value reported here. However, these effects are not expected to change the comparative conclusion, because all three architectures were evaluated under the same load basis, and the battery remains essential for removing repeated startup and transient deficits.

Therefore, the PEMFC + PV + Battery architecture is selected as the preferred reference configuration for the next experimental EMS validation phase. Future work will replace the ideal converter efficiencies with measured values and extend the model to include converter dynamics, PEMFC transient response, measured battery behaviour, hydrogen-flow dynamics, and experimental validation on the prototype platform, linking the simulation results of this paper with measured prototype performance.

References

1. Balestra, L. and Schjølberg, I., 2021. Modelling and simulation of a zero-emission hybrid power plant for a domestic ferry. *International Journal of Hydrogen Energy*, 46(18), pp.10924–10938.
2. Bassam, A.M. et al., 2023. A solar energy-based shore-side power system for a ferry service across the Suez Canal.
3. Cha, M. et al., 2021. Power management optimisation of a battery/fuel cell hybrid electric ferry. In: *Proceedings of the 2021 31st Australasian Universities Power Engineering Conference (AUPEC 2021)*. Institute of Electrical and Electronics Engineers Inc. Available at: https://doi.org/10.1109/AUPEC52110.2021.9597787
4. IMO, 2023. *2023 IMO Strategy on Reduction of GHG Emissions from Ships*. Available at: https://www.imo.org/en/OurWork/Environment/Pages/2023-IMO-Strategy-on-Reduction-of-GHG-Emissions-from-Ships.aspx (Accessed: June 29, 2025).
5. Kumar, P.S. and Kanimozhi, T., 2024. Hybrid PV and fuel cell generating system for shipboard applications based on optimal dispatch evaluator algorithm. *Journal of Advanced Research in Applied Sciences and Engineering Technology*, 36(2), pp.131–146. Available at: https://doi.org/10.37934/araset.36.2.131146
6. PVGIS, 2026. *PVGIS 5.3 solar panel calculator*. Available at: https://pvgis.com/en/pvgis-5-3 (Accessed: May 11, 2026).
7. Ringel, M. et al., 2024. Green hydrogen cooperation between Egypt and Europe: The perspective of locals in Suez and Port Said. *International Journal of Hydrogen Energy*, 79, pp.1501–1510. Available at: https://doi.org/10.1016/j.ijhydene.2024.06.239
8. Vahabzad, N., Mohammadi-Ivatloo, B. and Anvari-Moghaddam, A., 2021. Optimal energy scheduling of a solar-based hybrid ship considering cold-ironing facilities. *IET Renewable Power Generation*, 15(3), pp.532–547. Available at: https://doi.org/10.1049/rpg2.12015
9. Zhaka, V. and Samuelsson, B., 2024. Hydrogen as fuel in the maritime sector: From production to propulsion. *Energy Reports*, pp.5249–5267. Available at: https://doi.org/10.1016/j.egyr.2024.11.005
10. Zumbraegel, T. and Kegel, A., 2025. Green tides: The Suez Canal as key hub and green corridor for a hydrogen future between the Middle East and Europe. *Frontiers in Energy Research*, 13. Available at: https://doi.org/10.3389/fenrg.2025.1538792

Aya A. ElBauomy is a Marine Engineer, Teaching Assistant, and Researcher at the Arab Academy for Science, Technology and Maritime Transport (AASTMT), Alexandria, Egypt. She is currently a PhD candidate with research interests in hydrogen-based marine energy systems, hybrid ship propulsion, maritime decarbonisation, and the reduction of ship emissions. She holds a Master's degree in Climate Change in Maritime Studies, with a research focus on sustainable maritime technologies and low-emission ship energy systems.

Dr. Gintvilė Šimkonienė is affiliated with the Department of Engineering, Faculty of Marine Technology and Natural Sciences, Klaipėda University, Lithuania, where she also serves as Vice-Dean for Research and International Relations. Her academic and research interests are related to electrical power engineering, renewable energy systems, energy-system reliability, distribution-grid reliability, and the integration of renewable energy resources. Her work also covers applied engineering research and sustainable energy technologies, including solar power systems and their reliability and safety challenges.

Prof. Mostafa Ahmed Abdelgeliel is a Professor of Electrical and Control Engineering at the Arab Academy for Science, Technology and Maritime Transport, Alexandria, Egypt. His research focuses on automatic control, fault detection and fault-

tolerant systems, process control, renewable energy systems, photovoltaic plants, and optimal operation of multi-source generation systems.

Dr. Kareem M. Tonbol is an Associate Professor of Physical Oceanography and Climatology at the Arab Academy for Science, Technology and Maritime Transport, Alexandria, Egypt. His research focuses on physical oceanography, climate change, sea level rise, coastal systems, meteorological and oceanographic data analysis, and climate modeling.

PEMFC–BATERIJOS–PV HIBRIDINIŲ ARCHITEKTŪRŲ GALIOS PUSIAUSVYROS VERTINIMAS PROTOTIPINIAM KATAMARANUI REMIANTIS REALAUS MARŠRUTO EKSPLOATAVIMO SCENARIJUMI

Aya A. ElBauomy, Gintvilė Šimkonienė, Mostafa Ahmed Abdelgeliel, Kareem M. Tonbol

Jūrų transporto dekarbonizacijai būtinos mažų emisijų ir dinamiškai prisitaikančios, trumpiems, pasikartojantiems maršrutams tinkamos varymo sistemos. Šiame straipsnyje pateikiamas maršrutu grįstas, laiko srityje atliktas protonų mainų membraniniais kuro elementais (PEMFC) pagrįstų hibridinių architektūrų galios balanso vertinimas, skirtas 1,80 m ilgio prototipiniam katamaranui.

Reali kelto eksploatavimo situacija Sueco kanalo regione buvo transformuota į reprezentatyvų 15 minučių trukmės prototipo darbo ciklą, kuris kartojamas per 8 valandų eksploatacijos laikotarpį. Vertinti trys atvejai, naudojant tą pačią nuolatinės srovės (DC) magistralės apkrovą:(1) PEMFC + akumuliatorius;(2) PEMFC + fotovoltinė sistema (FV); (3) PEMFC + FV + akumuliatorius.

PEMFC ir akumuliatoriaus veikimas modeliuotas remiantis DC magistralės galios balansais, keitiklio, akumuliatoriaus srovės ir įkrovos būsenos (SOC) lygtimis. FV sistemos indėlis apskaičiuotas taikant laivo fotovoltinės galios modelį, naudojant PVGIS sezoninės saulės spinduliuotės ir temperatūros duomenis.

Rezultatai parodė, kad pirmuoju atveju užtikrinamas pereinamųjų paleidimo galios trūkumų kompensavimas pasitelkiant akumuliatorių, tuo tarpu antruoju atveju sumažinama PEMFC apkrova, tačiau be energijos kaupiklio nepašalinami paleidimo metu atsirandantys galios deficitai. Esant palankiausioms sezoninėms sąlygoms liepą, FV sistemos didžiausia galia siekė 84,88 W, o antrojo atvejo FV pagaminta energija sudarė 399,64 Wh.

Trečiuoju atveju FV energijos panaudojimas DC magistralėje padidėjo iki 450,87 Wh, galutinė akumuliatoriaus įkrovos būsena išliko aukšta (SOC = 0,90), o pasikartojantys pereinamieji galios trūkumai buvo pašalinti, laikantis idealių galios balanso prielaidų.

Remiantis šiais rezultatais, PEMFC + FV + akumuliatoriaus hibridinė architektūra identifikuojama kaip optimali konfigūracija tolimesniam eksperimentinio prototipo vystymo etapui.

Pagrindiniai žodžiai: PEMFC; akumuliatorius; fotovoltinė sistema; hibridinė varomoji jėga; nuolatinės srovės magistralės galios balansas